The initial conditions and mission state in the retrieval case are set, respectively, by the following equations:

$$l_0 = 100 \text{ km}, \quad \dot{\Theta}_0 = 5.73 \times 10^{-3} \text{ deg/min},$$

$$\dot{l}_0 = \Theta_0 = \phi_0 = \dot{\phi}_0 = 0 \tag{10}$$

$$l_m = 1 \text{ km}, \quad \dot{l}_m = \Theta_m = \dot{\Theta}_m = \phi_m = \dot{\phi}_m = 0 \tag{11}$$

The time history during retrieval of the subsatellite is shown in Fig. 3. It takes about 170 min to accomplish the control objective. The tether length l in-plane rotation Θ and out-of-plane rotation ϕ are 0.365 km, 25.5 deg, and -0.755 deg, respectively, at that time.

V. Conclusions

The control problem of deployment and retrieval of the tethered subsatellite has been studied by using the mission function control.

The results of numerical simulation show that controllability of the mission function control is affirmed on the deployment and retrieval of the subsatellite connected to a main body through a tether swinging both in in-plane and out-of-plane motions. It is therefore concluded that the present control algorithm works quite well during this control problem when the three-dimensional motion of the tethered subsatellite is taken into account for the analysis.

References

[1]Misra, A. K., and Modi, V. J., "Dynamics and Control of Tether Connected Two-Body Systems—A Brief Review," *Space 2000,* edited by L. G. Napolitano, AIAA, New York, 1983, pp. 473–514.

[2]Fujii, H., and Ishijima, S., "The Mission Function Control for Deployment and Retrieval of a Subsatellite," *Journal of Guidance, Control, and Dynamics,* Vol. 12, No. 2, March-April 1988, pp. 243–247.

[3]Misra, A. K., and Modi, V. J., "Dynamics of a Tether Connected Payload Deploying from the Space Shuttle," *Second VPI&SU/AIAA Symposium on Dynamics and Control of Large Flexible Spacecraft,* Virginia Polytechnic Inst. and State Univ., Blacksburg, VA, June, 1979.

Fast Orbit Propagator for Graphical Display

F. Landis Markley* and James F. Jeletic†
NASA Goddard Space Flight Center, Greenbelt, Maryland 20771

Introduction

IT is often desirable to provide a graphical display of spacecraft orbits, either as ground tracks on flat maps or as paths on perspective views of the globe. The resolution of wall displays or personal computer screens does not demand the accuracy provided by a sophisticated orbit propagator, and so a fast, simple, analytic two-body propagator is suitable. Naive applications of analytic propagators that ignore the distinction between mean and osculating Keplerian elements can lead to large intrack errors. We present a simple analytic orbit propagator incorporating a mean-to-osculating transformation and study its errors in a numerical example.

Received May 24, 1989; revision received Aug. 22, 1989.

*Head, Control System Software and Simulation Section. Associate Fellow AIAA.

†Software Engineer, Advanced Technology Section.

Formulation

An extended-time, zeroth order theory[1] computes orbits with sufficient accuracy for our purpose. That is, in propagating an orbit from time t_0 to time t, we can tolerate errors of order J_2, but not of order $J_2(t - t_0)$. This means that we must compute the secular perturbations and the semimajor axis (which affects the mean motion) to first order in J_2, but we can ignore other orbit perturbations. The transformations between Cartesian elements and osculating Keplerian elements are standard, so the orbit propagation problem is to compute the osculating Keplerian elements at time t in terms of the osculating Keplerian elements at time t_0. This proceeds in three steps: conversion of osculating to mean Keplerian elements at time t_0, propagation of the mean elements from t_0 to t, and conversion of mean to osculating Keplerian elements at time t.

Consider the propagation of the mean elements first. Denoting the Brouwer mean elements by overbars and retaining only the secular terms in J_2, we find that the semimajor axis $\bar{a}$, eccentricity $\bar{e}$, and inclination $\bar{i}$ are constant, and that[2]

$$\bar{\omega}(t) = \bar{\omega}(t_0) + (3/2)J_2R^2p^{-2}\bar{n}[2 - (5/2)\sin^2\bar{i}](t - t_0) \tag{1}$$

$$\bar{\Omega}(t) = \bar{\Omega}(t_0) - (3/2)J_2R^2p^{-2}\bar{n}\cos\bar{i}(t - t_0) \tag{2}$$

$$\bar{M}(t) = \bar{M}(t_0) + \bar{n}(t - t_0) \tag{3}$$

where

$$p \equiv \bar{a}(1 - \bar{e}^2) \tag{4}$$

$$\bar{n} = \sqrt{\mu/\bar{a}^3}[1 + (3/2)J_2R^2p^{-2}(1 - \bar{e}^2)^{1/2}(1 - (3/2)\sin^2\bar{i})] \tag{5}$$

In these equations, R is the equatorial radius of the Earth, used only for scaling J_2, and μ is the Earth's gravitational constant. It is convenient to define a new "mean" semimajor axis $\hat{a}$ by

$$\hat{a} \equiv \bar{a}[1 - J_2R^2p^{-2}(1 - \bar{e}^2)^{1/2}(1 - (3/2)\sin^2\bar{i})] \tag{6}$$

since this and Eq. (5) give

$$\bar{n} = \sqrt{\mu/\hat{a}^3} \tag{7}$$

to first order in J_2. Note that $\hat{a}$, like $\bar{a}$, is independent of time. We can also replace p in Eq. (1) and (2) by

$$\hat{p} \equiv \hat{a}(1 - \bar{e}^2) \tag{8}$$

since p (the semilatus rectum) only appears in terms already first order in J_2 in these equations. Thus, the propagation of the mean elements is given by Eq. (3),

$$\bar{\omega}(t) = \bar{\omega}(t_0) + (3/2)J_2R^2\hat{p}^{-2}\bar{n}(2 - 5/2)\sin^2\bar{i}](t - t_0) \tag{9}$$

$$\bar{\Omega}(t) = \bar{\Omega}(t_0) - (3/2)J_2R^2\hat{p}^{-2}\bar{n}\cos\bar{i}(t - t_0) \tag{10}$$

Now consider the conversion of mean to osculating elements at time t. We can ignore the difference between mean and osculating values of all Keplerian elements except the semimajor axis because the errors introduced by this approximation are of order J_2. However, we must compute the mean-to-osculating transformation of the semimajor axis to order J_2 because an order J_2 error in the semimajor axis would give, through Eq. (7), an order J_2 error in the mean motion $\bar{n}$, and thus, an error of order $J_2(t - t_0)$ in the orbit. The difference between the mean and osculating semimajor axis is a short-period term (Ref. 2, p. 288),

$$a = \bar{a} + (J_2R^2/a)\{(1 - (3/2)\sin^2 i)[(a/r)^3 - (1 - e^2)^{-3/2}] + (3/2)(a/r)^3\sin^2 i\cos 2(f + \omega)\} \tag{11}$$

Table 1 Results of the propagation runs in one day increments starting at the orbit vector epoch time

Time[a] dpYYY:MM:DD:HH:MM:SS		GMAS 15×15	GMAS 4×4	Fastorb	OrbJ2
1989:06:01:00:00:00	Longitude	110.54	110.54	110.55	110.55
	Latitude	0.00	0.00	0.00	0.00
1989:06:02:00:00:00	Longitude	92.54	92.51	90.22	92.46
	Latitude	−5.67	−5.70	−6.92	−5.74
1989:06:03:00:00:00	Longitude	74.35	74.25	69.51	74.16
	Latitude	−11.15	−11.20	−13.49	−11.27
1989:06:04:00:00:00	Longitude	55.76	55.57	48.12	55.46
	Latitude	−16.23	−16.31	−19.32	−16.40
1989:05:05:00:00:00	Longitude	36.62	36.31	25.79	36.18
	Latitude	−20.70	−20.90	−24.02	−20.90
1989:06:06:00:00:00	Longitude	16.84	16.37	2.53	16.25
	Latitude	−24.33	−24.45	−27.17	−24.53
1989:06:07:00:00:00	Longitude	356.44	355.80	338.63	355.69
	Latitude	−26.92	−27.02	−28.48	−27.08
1989:06:08:00:00:00	Longitude	335.61	334.77	314.65	334.67
	Latitude	−28.28	−28.32	−27.77	−28.36

[a]Greenwich mean time.

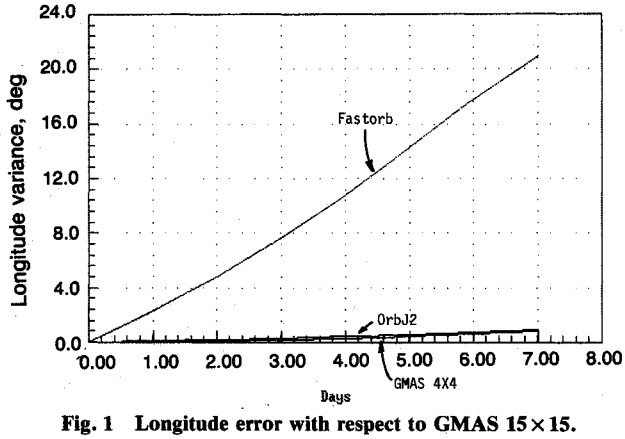

Fig. 1 Longitude error with respect to GMAS 15×15.

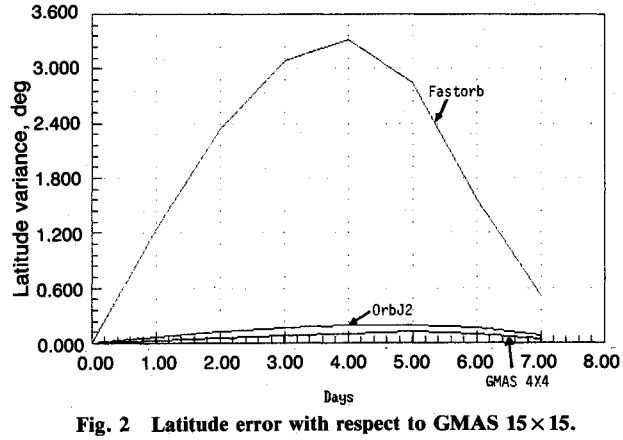

Fig. 2 Latitude error with respect to GMAS 15×15.

where r is the distance of the spacecraft from the center of the Earth, f is the true anomaly, and a (without an overbar) denotes the osculating semimajor axis. Time arguments are omitted from Eq. (11) because all time-dependent quantities are evaluated at the same time. As stated previously it is not necessary to distinguish between mean and osculating quantities other than $\bar{a}$ and a in this equation. Using Eq. (6) and

$$r = a(1 - e^2)/(1 + e\cos f) \tag{12}$$

we can see after some algebra that Eq. (11) is equivalent to

$$a(t) = \hat{a} + J_2R^2g(t)/\hat{a} \tag{13}$$

to first order in J_2, where

$$g(t) \equiv [(1 + e\cos f)/(1 - e^2)]^3[1 - 3\sin^2 i \sin^2(f + \omega)] \tag{14}$$

The time dependence of $g(t)$ comes from the time-dependent argument of perigee ω and true anomaly f.

The conversion of osculating elements to mean elements at time t_0 is the inverse of this. Again, we ignore differences between mean and osculating values of all the elements except the semimajor axis. Equation (13) is a quadratic equation for $\hat{a}$ that we solve exactly, rather than just to first order in J_2, to avoid a jump of order J_2^2 in the orbit for t infinitesimally greater than t_0. The physically significant root of the quadratic is

$$\hat{a} = (1/2)\{a(t_0) + [a^2(t_0) - 4J_2R^2g(t_0)]^{1/2}\} \tag{15}$$

To summarize, the orbit propagator uses Eqs. (14) and (15) at t_0 and Eqs. (3), (7-10), (13), and (14) at all other times t. The usual conversions between Cartesian and osculating Keplerian elements and between mean and true anomaly are also used.

Results

A nominal orbit for the Hubble Space Telescope was used to compare the errors of this orbit propagator with those of other propagators. In particular, the following orbit vector was used:

Semimajor axis	=	6970.78 km
Eccentricity	=	0.00001
Inclination	=	28.5 deg
Argument of perigee	=	0.0
Right ascension of ascending node	=	0.0
Mean anomaly	=	0.0

The selected scenario required a run over a one week period starting at the orbit vector epoch on June 1, 1989 at 0 h Greenwich mean time and ending on June 8, 1989, at 0 h using a 60 s propagation step interval. The four propagation models and algorithms used are as follows:

1) GMAS 15 × 15—a complex Cowell integration[3] with 15 × 15 geopotential field, gravitational perturbations due to the sun and moon, and atmospheric drag with ballistic coefficient 78.6 kg/m^2.

2) GMAS 4 × 4—a simple Cowell integration with 4 × 4 geopotential field, no third-body perturbations, and no atmospheric drag.

3) OrbJ2—a personal computer version of the two-body propagator described in this paper.

4) Fastorb—a personal computer-based algorithm similar to OrbJ2 but omitting the mean-to-osculating transformation of the semimajor axis.

The results of these runs are included in Table 1 and Figs. 1 and 2. The intrack, or longitude, error is clearly the dominant error. The error in GMAS 4 × 4 and OrbJ2 is due to the neglect of drag; the larger error in Fastorb is due to the error of order J_2 in the computation of the mean motion.

As an example of the resolution available in computer displays, we consider the IBM Enhanced Graphics Adaptor (EGA) board, which is widely used in personal computers. The resolution of the EGA board is 640 × 350 pixels (horizontal by vertical). Given that the entire world map is displayed (i.e., − 180° longitude to 180° longitude and − 90° latitude to 90° latitude) the number of pixels per degree of longitude is

$$(640/360) = 1.78 \text{ pixels/longitude degree}$$

and the number of pixels per degree of latitude is

$$(350/180) = 1.94 \text{ pixels/latitude degree}$$

In the case of this orbit scenario, the position of the Hubble Space Telescope after one week using OrbJ2 orbit propagator would have an error of

0.94° longitude = 1.67 pixels = 0.26% of the world map width
0.08° latitude = 0.16 pixels = 0.04% of the world map height

Note that these graphics screen errors are with respect to the position of the spacecraft subsatellite point. If a zoom is applied to the world map projection, the pixel and screen error becomes greater. In any case, the errors are quite acceptable for graphical display.

Conclusions

A fast, simple, analytic orbit propagator has been developed and shown to give acceptable results for the graphical display of the trajectories of Earth-orbiting satellites. First-order effects of the oblateness of the Earth on the orbit are included in a consistent manner. In particular, the propagator includes a mean-to-osculating transformation on the semimajor axis because large intrack errors can result from ignoring the distinction between mean and osculating values of this parameter.

Acknowledgment

The authors would like to thank Bob Dasenbrock of the U.S. Naval Research Laboratory for explaining the large intrack errors in analytic orbit theories that ignore the distinction between mean and osculating elements.

References

[1]Breakwell, J. V., and Vagners, J., "On Error Bounds and Initialization in Satellite Orbit Theories," *Celestial Mechanics*, Vol. 2, No. 2, 1970, pp. 253-264.

[2]Roy, A. E., *Orbital Motion*, Adam Hilger, Bristol, England, UK, 1982.

[3]Cappelari, J. O., Jr., Velez, C. E., and Fuchs, A. J. (eds.), *Mathematical Theory of the Goddard Trajectory Determination System*, NASA-X-582-76-77, April 1976.

Adaptive Noise Models for Extended Kalman Filter

K. Kumar,* D. Yadav,† and B. V. Srinivas‡
Indian Institute of Technology, Kanpur, 208 016 India

Introduction

KALMAN filters are sensitive to modeling errors as well as input statistics.[1-3] The danger of degradation in numerical performance is associated with the weakening/loss of positive definiteness of state covariance, leading to poorer predictions. The problem is further aggravated by measurement bias and relatively large errors in the starting state estimates.[4,5] Here, an attempt is made to develop a "global" extended Kalman filter by introducing some suitable adaptive driving noise covariance models. Numerical simulation of the problem of satellite orbit estimation from observational data using this filter with the proposed noise models clearly establishes their efficacy.

To combat the filter divergence, it is necessary to adopt schemes that ensure positive definiteness of the state covariance matrix and prevent it from "diminishing too rapidly."

Several trial and error approaches incorporating varying amounts of fictitious driving noise have been propsed[4,6]; however, these normally require a large number of simulation trials. Furthermore, the success of the filter is strongly dependent on errors in the initial state estimates assumed, thus leaving a degree of unpredictability regarding the filter convergence. Here, attention is focused on developing the noise models that would ensure filter convergence irrespective of the initial state estimate errors to the extent possible.

Adaptive State Noise Models

The models proposed here are dependent on some suitable measures of the state errors. These measures are taken to be residuals that are nothing but the differences between the actual observation values and their corresponding numerically "computed" projections. Numerous schemes were tried, of which only some are presented. Efficacy of the proposed models is tested through a problem of satellite orbit determination using an extended Kalman filter algorithm. The noise models presented here can be classified into two broad categories, as discussed in the following.

Noise Models Based on Observation Residuals

Here, we assume the driving noise covariance matrix Q to be diagonal; it is constructed using the observation residual statistics. It was felt that the diagonal terms should be taken so as to represent the level of dispersion in the corresponding observations. To account for systematic modeling errors, on the other hand, a certain degree of dependence of these terms on the means of observations also appears natural. It is therefore proposed to develop models with diagonal entries in Q based on the means as well as the standard deviations of the observation residuals. This has been incorporated such that an increase in systematic errors, reflected by enlarged mean errors, promotes fading memory, whereas the growth in the standard deviation induces expanding filter memory. It is therefore hoped that the following models proposed here would pave the way for adaptive filter characteristics.

Presented as IAF Paper 88-305 at the 39th IAF Congress, Bangalore, India, Oct. 1988; received Aug. 3, 1989; revision received Nov. 1, 1989.

*Professor, Department of Aerospace Engineering. Associate Fellow AIAA.
†Assistant Professor, Department of Aerospace Engineering.
‡Former Graduate Student, Department of Aerospace Engineering.